DOI: 10.26599/FSHW.2024.9250142

Y.M. Tian et al. / Food Science and Human Wellness 14 (2025)

Contents lists available at SciOpen

Food Science and Human Wellness

journal homepage: https://www.sciopen.com/journal/2097-0765

Simultaneous quantification of trace heavy metals in mushrooms using a three-dimensional highly reduced graphene oxide/Fe_3O_4 nanocomposite-based electrochemical sensor

Yiming Tian[1#], Pingsheng Zhong[1#], Kai Zhou[1], Lufei Zheng[2], Jiali Ren[1]*

[1] *Hunan Key Laboratory of Forestry Edible Resources Safety and Processing, Hunan Key Laboratory of Grain-oil Deep Process and Quality Control, Central South University of Forestry and Technology, Changsha, 410004, China.*

[2] *Institute of Quality Standard and Testing Technology for Agro-Products of CAAS, Beijing, 10081, P. R. China*

ABSTRACT: The accumulation of heavy metals in mushrooms has presented a significant risk to human health, underscoring the importance of devising a portable and cost-effective method for detecting heavy metals. Thus, we have developed an electrochemical sensor based on 3-dimensional highly reduced graphene oxide (3D-HRGO) in conjunction with Fe_3O_4 nanoparticles, enabling the simultaneous quantification of Cd^{2+}, Pb^{2+}, Cu^{2+}, and Hg^{2+}. The 3D-HRGO/Fe_3O_4 nano-particles material prepared in this study was characterized and confirmed by multiple techniques, then dispersed in a simple and environmental dispersant, consist of 75% ethanol and 0.1% Nafion, and coating on a glass carbon electrode (GCE) to preparing a 3D-HRGO/Fe_3O_4/GCE sensor. The limit of detection (LOD) of 3D-HRGO/Fe_3O_4/GCE sensor for Cd^{2+}, Pb^{2+}, Cu^{2+}, and Hg^{2+} in simultaneous detection were 0.2 μg/L, 0.6 μg/L, 0.6 μg/L, and 0.9 μg/L, respectively. The sensor demonstrates exceptional stability, reproducibility, anti-interference, and recovery rate. Furthermore, the electrochemical sensor was employed to detect heavy metals in actual mushrooms and validated through conventional methodologies. This study represents the pioneering utilization of 3D-HRGO/Fe_3O_4 as a foundational material for an electrochemical sensor capable of simultaneous detection of multiple metals, thereby advancing the progress of on-site and expeditious detection techniques.

Keywords: Electrochemical sensor; 3D-HRGO/Fe_3O_4 nanocomposite; mushrooms; heavy metals; rapid and simultaneous detection

1. Introduction

Edible mushrooms are widely consumed worldwide due to their nutritional value and palatability. However, their growth process makes them susceptible to the accumulation of heavy metals from the environment, which can have detrimental effects on human health, such as osteoporosis, rickets, and dwarfism[1-3]. Various conventional analytical techniques, including atomic absorption spectrometry (AAS)[4-6], inductively coupled plasma-optical emission spectrometry (ICP-OES)[7, 8], and ICP-MASS spectrometry[9], are commonly employed for the detection and quantification of heavy metal ions. Although these analytical methods possess remarkable stability, precision, and low detection limits, their lack of universalization and portability is attributed to the bulky and costly instruments employed. Consequently,

#contributed equally to this work.
***Corresponding author**
Jiali Ren (J. L. Ren), E-mail: t20091483@csuft.edu.cn

Received 26 August 2023
Received in revised from 12 September 2023
Accepted 5 December 2023

there is an urgent need to develop more convenient, cost-effective, and portable techniques that enable on-site detection of heavy metals.

The electrochemical sensor possesses several advantageous characteristics, including high sensitivity, rapid response time, and low cost[10]. The advancement of micro-electro-mechanical system (MEMS) technology has further facilitated the creation of portable electrochemical instruments, enabling real-time detection while minimizing energy consumption[11]. To enhance the sensor's detection capabilities, such as the detection limit, stability, and reproducibility, a chemically modified electrode was employed[12, 13]. However, the attributes of electrode-modifying materials, including electron transport efficiency, specific surface area, catalytic properties, and adsorption capabilities, play a crucial role in determining the performance of modified electrodes[14]. Therefore, it has been a significant surge in research interest surrounding the development of novel functional materials for modified electrodes.

Graphene (GR) is called “smart material”[15] due to its excellent physical and chemical properties[16, 17], including ultra-high specific surface area and a strong conductivity ($\sigma \approx 10^6$ S/m)[18, 19]. However, some disadvantages such as susceptibility to van der Waals force frangibility and hydrophobicity hinder its application as an electrochemical sensor material[20-22]. 3D-graphene and graphene/metal oxide composite have been studied to surmount those shortages[23, 24]. Furthermore, the combination of metal oxide nanoparticles and graphene yields synergistic effects that significantly enhance the electrochemical properties of nanocomposites[25]. Specifically, Fe_3O_4 nanoparticles have been identified as a highly effective material for enhancing the performance of electrochemical sensors due to their favorable catalytic, electrical, and adsorptive properties. Extensive research has demonstrated that the incorporation of Fe_3O_4 nanoparticles with graphene results in even more remarkable detection performance[26, 27].

In this study, a novel electrochemical sensor based on 3D-HRGO/Fe_3O_4/GCE was developed for the simultaneous detection of heavy metals using the differential pulse anodic stripping voltammetry (DPASV) technique. This is the first study where the 3D-HRGO was applied for the electrochemical sensor construction and simultaneous detecting four heavy metal ions in different mushrooms. In addition, the excellent abilities of conductivity and specific surface area were kept for the 3D-HRGO material. Moreover, the simple and environmental dispersant composed of 75% ethanol-0.1% Nafion was first applied to dispersing super hydrophobic 3D-HRGO/Fe_3O_4. The sensor was successfully employed to detect Cd^{2+}, Pb^{2+}, Cu^{2+}, and Hg^{2+} in edible mushrooms, and the results were validated using the atomic absorption spectroscopy (AAS) method. The findings demonstrate that the proposed electrochemical method, based on the 3D-HRGO/Fe_3O_4 nanocomposite, exhibits exceptional performance in terms of repeatability, reproducibility, anti-interference capability, and detection limit.

2. Materials and methods

2.1 Chemicals reagents and apparatus

The reduced graphene oxide (RGO) was procured from Chengdu Organic Chemical Co., Ltd. Standard ion solutions of Cd^{2+}, Pb^{2+}, Cu^{2+}, and Hg^{2+} for quantification were obtained from Guobiao (Beijing) Testing &

Certification Co., Ltd. The Nafion solution was acquired from Sigma-Aldrich. All mushroom samples were obtained from local markets. Unless specified otherwise, all other chemicals and reagents used were of analytical grade. All solutions were prepared using ultra-pure water (Resistivity≥18.25 MΩ·cm).

All of the electrochemical experiments were performed on an electrochemical workstation (CHI 920D, Shanghai Chenhua Instrument Co., Ltd., China). A system of three electrodes consisting of GCE (working electrode), platinum electrode (Pt, assistant electrode), and Ag/AgCl electrode (reference electrode) was purchased from Shanghai Chenhua Instrument Co., Ltd. The scanning electron microscope (SEM, Zeiss Sigma HD) was used to characterize the morphology of nanomaterials, Raman Spectrometer (Thermo Fisher Scientific), Fourier transform infrared spectrum (FTIR, Shimadazu, Japan), and x-ray photoelectron spectrum (XPS, Zeiss Sigma HD) were used to characterize the structure and elemental composition of nanocomposites.

2.2 Preparation of 3D-HRGO/Fe_3O_4/GCE electrode

2.2.1 Fabrication of 3D-HRGO/Fe_3O_4

The preparation of 3D-HRGO/Fe_3O_4 was described as Scheme 1[28, 29].

Step 1: 200 mg of RGO was dispersed in 200 mL of water through the process of sonication for a duration of 15 min. Ethanol was then gradually added until the RGO was fully dispersed. Following this, 6.0 mL of 80% dimethylhydrazine was added dropwise while stirring, and sonication was continued for an additional 15 min. The resulting RGO dispersion was subsequently transferred into a Teflon-lined high-pressure reaction kettle and preheated in a muffle furnace at a temperature of 100℃ for a duration of 1 h. Then, the temperature was increased to 180℃ and maintained for a period of 24 h. Cooling, the product was washed and finally freeze-dried to obtain 3D-HRGO.

Step 2: 100 mg 3D-HRGO was dispersed in 100 mL water. Subsequently, 20 mL of a 0.01 M $FeCl_3 \cdot 6H_2O$ solution and 40 mL of a 0.02 M sodium citrate solution were gradually added to the 3D-HRGO dispersion while stirring. The mixture was then transferred to a high-pressure reaction kettle and subjected to heating at 180℃ for a duration of 12 h in a muffle furnace. After cooling, the products were thoroughly washed with deionized water, separated in the presence of an external magnetic field, and subsequently subjected to freeze-drying to obtain 3D-HRGO/Fe_3O_4. The graphene oxide (GO) was synthesized using the Hummer method[30].

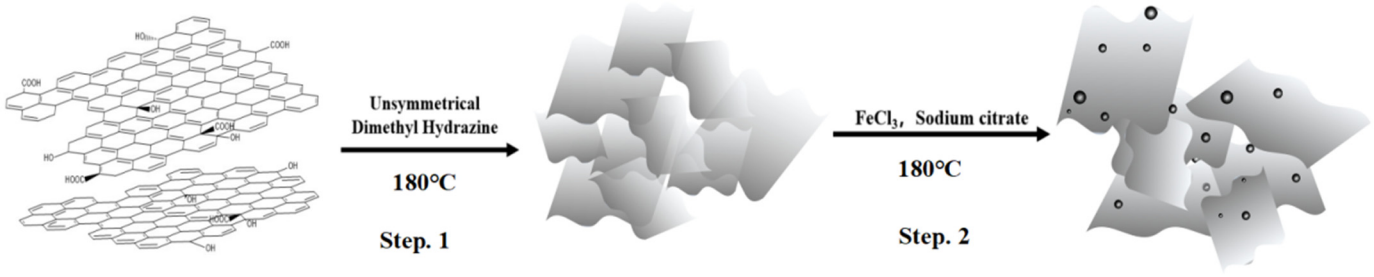

Scheme 1. Preparation of 3D-HRGO/Fe_3O_4 nanocomposite material.

2.2.2 Characterization of nanomaterials

The materials mentioned above, including GO, RGO, 3D-HRGO, and 3D-HRGO/Fe_3O_4, were subjected to various characterization techniques in this study. The morphology of these materials was examined by using SEM with a 10 kV landing voltage, while the elemental composition was analyzed by using the XPS equipped in the SEM, and the energy for scanning ranges from 0 to 5 keV, and all data for analyzed elements has been normalized. The Raman spectroscopy was applied to evaluate the mono-layer characteristic and scanning from 0 to 3500 cm^{-1}. The measurement of functional groups was conducted by using the FTIR, scanning range (400 – 4000) cm^{-1}. It is important to note that the magnetic nature of 3D-HRGO/Fe_3O_4 necessitated demagnetization before SEM analysis. Additionally, the SEM instrument used in this study was equipped with an XPS function unit for elemental analysis. The FTIR measurements of the fabricated materials were performed using the potassium-adsorption ratio bromide pellet technique.

2.2.3 Preparation of 3D-HRGO/Fe_3O_4/GCE

The GCE was subjected to careful polishing on a suede with alumina slurry (particle sizes of 1.0 μm, 0.3 μm, and 0.05 μm in sequential order). Then washed with deionized water and ethanol, and dried in air. The 3D-HRGO/Fe_3O_4 material was dispersed in 75% ethanol containing 0.1% Nafion and subjected to sonication for 60 min to obtain a suspension. Finally, 30 μL suspension was coated on the surface of GCE and dried in the air to gain a modified electrode.

2.3 Electrochemical determination

2.3.1 The characterization of 3D-HRGO/Fe_3O_4 /GCE electrochemical abilities

The electrochemical experiments of 3D-HRGO/Fe_3O_4/GCE including cyclic voltammetry (CV), electrochemical impedance spectroscopy (EIS), electrode polarization curve, and optimization of detection conditions were carried out by CHI 920D electrochemical workstation. All of the experiment data were processed in Origin software.

2.3.2 Quantification of trace Cd^{2+}, Pb^{2+}, Cu^{2+} and Hg^{2+}using DPASV method

In order to obtain better detection results, all detection conditions have been optimized. To facilitate simultaneous and individual detection, a mixture of standard heavy metals ion solutions or digested solutions of real samples was prepared by combining them with 0.1 M PBS buffer in a 1:3 (v/v) ratio. This mixture was then added to a chemical testing cell. The deposition potential was set at -1.4 V, with a deposition time of 180 s. Stirring was employed during the deposition process, while the solution was kept still during stripping. Following each test, an electrode cleaning program was executed, involving a deposition potential of 0.3 V for 60 s. Additionally, the data obtained through the DPASV method were cross-validated using conventional AAS and atomic fluorescence spectrometry (AFS) techniques. PBS buffer containing 0.1 M Zn^{2+}, Ca^{2+}, Mg^{2+}, SO_4^{2-} and NO_3^-, respectively, was used to test the anti-interference ability of the electrochemical sensor for the detection of heavy metals.

2.4 Real Samples and Processing

Mushroom samples including *L. edodes*, *T. fuciformis*, and *A. blazei* were obtained from local markets and dried at 60°C for 24 h, then pulverized into powder. The digestion of all mushroom samples was carried out using the $HNO_3/HClO_4$ digestion method, with certain modifications made in accordance with the procedure outlined in reference[31]. 2.0 g sample powder was digested with 3 mL of HNO_3 and 3 mL of $HClO_4$ in a graphite digestion apparatus, until the resulting mixture was evaporated to a volume not exceeding 4 mL, then, 0.5 mol/L HCl was drop added till the digested solution turned to clarify, triplicate for each test. Finally, the replicates for each sample were combined and concentrated to a final volume of 10 mL. The digested sample solution was mixed with PBS at a ratio of 1:3 (v/v) for further detection.

3. Results and discussion

3.1 Characterization of 3D-HRGO/Fe_3O_4 nanocomposite

The performance of electrochemical sensors is notably affected by the structure and composition of nanomaterials, which can be readily characterized through spectroscopy and electrochemical techniques.

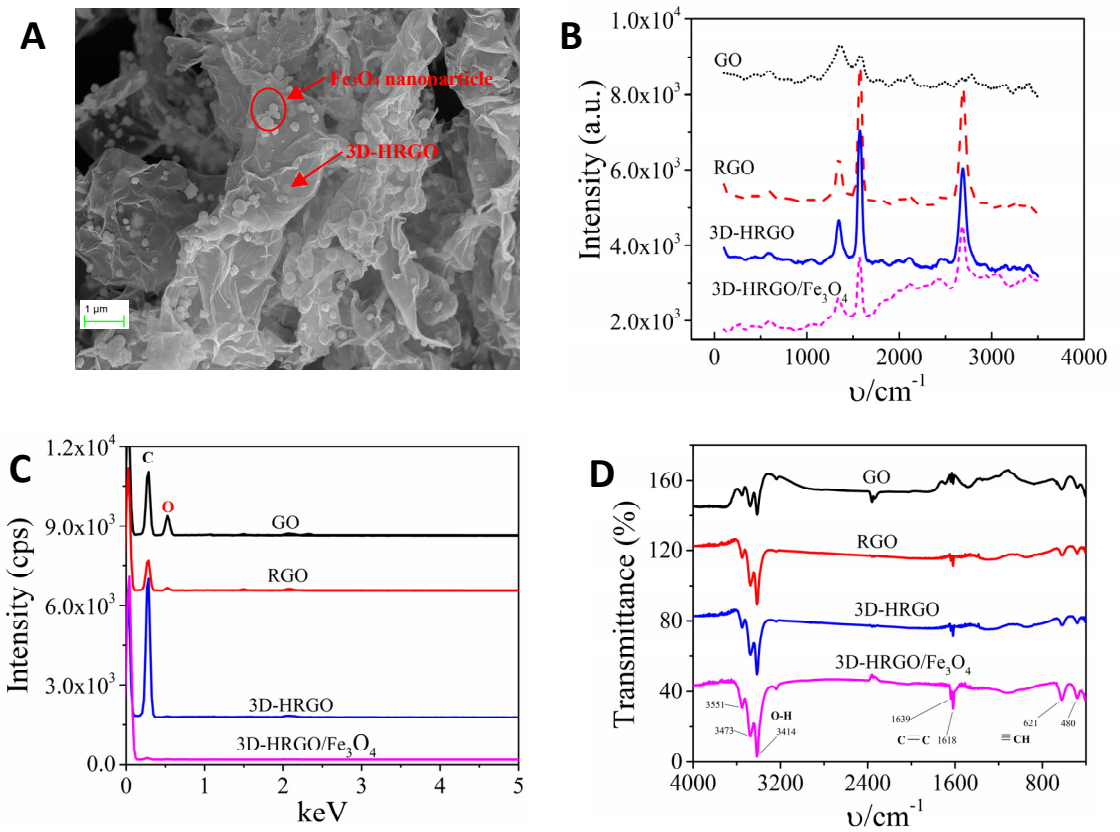

Fig. 1 The characterization of graphene and its composite nanomaterials. (A) SEM photographs of 3D-HRGO/Fe_3O_4; (B) Raman spectrum of GO, RGO, 3D-HGRO, 3D-HGRO/Fe_3O_4; (C) XPS spectrum of GO, RGO, 3D-HGRO, and 3D-HGRO/Fe_3O_4; (D) FTIR spectrum of GO, RGO, 3D-HGRO, 3D-HGRO/Fe_3O_4.

As shown in the SEM photograph where the 3D-HRGO/Fe_3O_4 forms a structure of folding, bending, and curling, and shows the nano-Fe_3O_4 particles well attached on the 3D-HRGO with diameters about (30 – 300) nm (see Fig. 1A, labeled with a red circle and pointed by an arrow) which helps to avoid the stacking of graphene sheets. In addition, the layer quality of graphene materials was identified by Raman spectroscopy[32]. The ratio of D/G (I_D/I_G) was applied to quantify the degree of disorder and it was calculated to be 1.36 for GO.

The I_D/I_G ratios of RGO and 3D-HRGO were determined to be 0.30 and 0.29, respectively, as shown in Fig. 1B. These values indicate that the carbon structures of RGO and 3D-HRGO possess fewer cavities and exhibit lower degrees of disorder compared to GO. Additionally, the I_D/I_G ratio of 3D-HRGO/Fe_3O_4 was found to be 0.32, which is close to the ratios observed for RGO and 3D-HRGO. This suggests that the introduction of nano-Fe_3O_4 particles as decoration does not disrupt the three-dimensional framework structure of 3D-HRGO. Furthermore, the number of graphene layers is correlated with the wave number υ, as depicted in Fig. 1B. Specifically, an increase in the number of layers leads to a red shift in the υ values of the G peaks, while the 2D peaks exhibit a blue shift. The wave numbers (υ) corresponding to the "G" peaks for GO, RGO, 3D-HRGO, and 3D-HRGO/Fe_3O_4 are measured to be 1582 cm^{-1}, 1575 cm^{-1}, 1573 cm^{-1}, and 1570 cm^{-1}, respectively. Similarly, the wave numbers (υ) associated with the "2D" peaks are found to be 2780 cm^{-1}, 2689 cm^{-1}, 2687 cm^{-1}, and 2682 cm^{-1}, respectively. These findings suggest that the 3D-HRGO/Fe_3O_4 nanocomposite exhibits remarkable characteristics of a single-layer material.

The presence of electron-withdrawing groups, which are oxygen-containing functional groups, grafted onto graphene oxide, has been found to reduce the efficiency of electron transfer[33]. The reduction of graphene can be assessed by analyzing the intensity of the C atomic and O atomic (I_C/I_O) ratio using XPS[34, 35]. In Fig. 1C, the I_C/I_O ratios for GO, RGO, 3D-HRGO, and 3D-HRGO/Fe_3O_4 are reported as 2.3, 8.4, 66.6, and 4.4, respectively (Fig. 1C). The I_C/I_O ratio of GO is found to be the lowest, primarily attributed to the presence of a significant number of oxygen-containing functional groups (-OH, -COOH, and -CHO) grafted onto its surface. These functional groups enhance the material's resistance, as evidenced by the electrochemical test depicted in Fig. 2A. Conversely, RGO exhibits an increased I_C/I_O value, indicating a lower concentration of oxygenated functional groups. Additionally, the I_C/I_O ratio of 3D-HRGO experiences a substantial increase when subjected to the strong reducing agent dimethylhydrazine. Conversely, the decrease in I_C/I_O observed in 3D-HRGO/Fe_3O_4 can be attributed to the presence of oxygen atoms within the Fe_3O_4 nanoparticles.

FTIR images (Fig. 1D) demonstrate that the 3D-HRGO/Fe_3O_4 has been highly reduced. A characteristic peak with strong absorption appears at 3400-3500 cm^{-1} for GO indicating -OH stretching vibration caused by water. The peak in positions of 1618 cm^{-1} and 1639 cm^{-1} is attributable to C=C stretching vibrations. Peaks located at 621 cm^{-1} were caused by ≡C-H stretching vibration. The peak of C=C, ≡C-H stretching vibration gradually increased from GO to 3D-HRGO/Fe_3O_4. The removal of electron-withdrawing oxygen-containing groups resulted in a significant enhancement in the electron transfer efficiency of the material. The presence of RCOO- and C-O groups was observed in the spectral range of 1500 cm^{-1} to 500 cm^{-1}, with the highest intensity observed in GO. Interestingly, there is no absorption peaks corresponding to Fe-O were detected in the range of 600 cm^{-1} to 500 cm^{-1}. This absence could be attributed to the low concentration of Fe_3O_4 and covered by 3D-HRGO, as evidenced by SEM analysis demonstrating clearly the combination of 3D-HRGO and Fe_3O_4.

3.2 Optimization of detection conditions for 3D-HRGO/Fe_3O_4/GCE

In order to adept the super-hydrophobic properties of 3D-HRGO/Fe_3O_4, it is crucial to carefully select appropriate dispersing agents. Generally, surfactants are usually used as a stabilizer to prevent graphene

sheets from coagulating but harmful to the environment[36, 37]. Thus, sodium dodecyl sulfate (SDS), N-methyl pyrrolidone (NMP), and ethanol have been considered as potential dispersing agents. However, the use of SDS as a dispersing agent leads to the generation of foam, preventing the formation of a uniform coating on the GCE. Similarly, NMP results in an unfavorable film formation. Fortunately, the utilization of a 75% ethanol aqueous solution as a dispersant exhibits superior properties in achieving the desired outcome.

The buffers and ionic strength play a crucial role in determining the electrochemical behavior exhibited by electrodes. Furthermore, the conductivity and mass transfer resistance have a discernible impact on the response signal generated by the electrochemical sensor. These factors necessitate the optimization of detection conditions, encompassing variables such as (A) the concentration of the 3D-HRGO/Fe_3O_4 dispersion, (B) the concentration of Nafion, (C) the utilization of different buffer systems, (D) the pH value, (E) the stirring speed, and (F) the deposition time. Supplementary materials (S.1) provide the relevant data and figures about the optimization process. The quantity of 3D-HRGO/Fe_3O_4 exhibits a direct correlation with the specific surface area, however, a substantial layer of material amplifies the hindrance to mass transfer. As a non-conductive polymer compound adhesive, the concentration of Nafion must be appropriately selected to ensure that Nafion not only adheres 3D-HRGO/Fe_3O_4 onto the electrode but also does not impact the resistance. Stirring serves to diminish concentration polarization and electric double-layer capacitance.

The following are the optimal detection conditions: (A) a concentration of 7 mg/mL for the 3D-HRGO/Fe3O4 dispersion; (B) a concentration of 0.1% for Nafion; (C) the use of PBS as the buffer system; (D) maintaining a pH of 5.0 for the PBS; (E) a deposition time of 180 s; and (F) a stirring speed of 1200 r/min.

3.3 Electrochemical behavior of 3D-HRGO/Fe_3O_4 nanocomposite based sensor

Electrochemical impedance spectroscopy (EIS) was used to evaluate the electrochemical behavior of the modified electrode (Fig. 2A, an equivalent circuit was inserted to explain the data of the EIS). The resistance of the system includes four parts: the solution resistance between working and reference electrodes (R_s), the double layer capacitance of electrodes and solution (C_d), Warburg impedance (Z_W), and electron transfer resistance (R_{ct}) caused by the obstruction of ions from solution to the interface. The electrochemical impedance spectroscopy (EIS) value R_{ct} of the GCE is measured to be 311 Ω, indicating that the transfer of electrons on the bare GCE is hindered by limited surface area. In contrast, the R_{ct} of the GO/GCE increases to 406 Ω due to the abundance of oxygen functional groups present on the GO surface. As previously mentioned, these oxygen-containing functional groups, known as electron-withdrawing groups, significantly diminish the electron transport efficiency of graphene oxide. The impedance of the electrode is influenced by two factors including oxygen-containing functional groups and mass transfer resistance. The same conclusion could be summarized from the comparison of RGO/GCE, 3D-RGO/GCE, and 3D-HRGO/Fe_3O_4/GCE. For the RGO/GCE containing less oxygen, the value of R_{ct} greatly decreases to 91 Ω. For the same reason, the R_{ct} of 3D-HRGO/GCE has a greatly further reduction to 15 Ω and the 3D-HRGO/Fe_3O_4/GCE has the lowest R_{ct} of 6 Ω.

The CV test was carried out and shown in Fig. 2B. The 3D-HRGO/Fe_3O_4/GCE got a much higher oxide and reduced response current than bare GCE. Firsty, compared to the bare GCE, the GO/GCE has much higher resistant (Fig. 2A), but larger specific surface area it has which provide more space for the transportation of electrons, those two effects lead to a equivalent response current for bare GCE and GO/GCE. While the reason for a stronger response signal obtained on RGO/GCE and 3D-HRGO/GCE is caused by the decreasing of resistance, obviously (see Fig. 2A). The synergy linking of Fe_3O_4 and 3D-HRGO makes it much easier for interface electron transfer[38, 39]. As it mentioned above, not only the capability of conductivity, but enormous specific surface area has 3D-HRGO remained. Furthermore, the Fe_3O_4 nano particles is a known inorganic metal oxide nanozymes which means it catalyzed the reduction of metal ions on the surface of 3D-HRGO/Fe_3O_4/GCE sensor and the activation energy required for this process is reduced and the decrease of electron transfer resistance leads to the increase of electron transfer efficiency, so the response current increases.

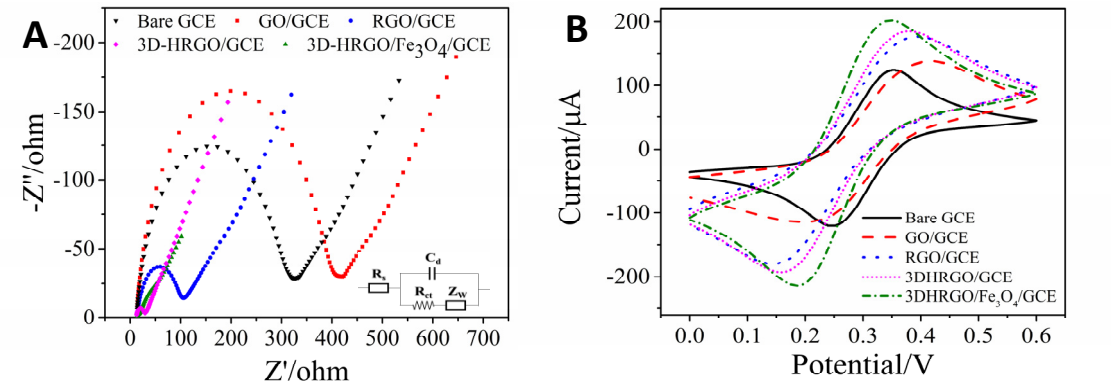

Fig. 2 The electrochemical behavior test for prepared electrochemical sensors. (A) EIS of bare GCE, GO/GCE, RGO/GCE, 3D-HRGO/GCE, and 3D-HRGO/Fe_3O_4/GCE in a 0.1 M PBS solution containing 5 mmol/L $[Fe(CN)_6]^{3-/4-}$ and 0.1 M KCl; (B) The CV of bare GCE, GO/GCE, RGO/GCE, 3D-HRGO/GCE, and 3D-HRGO/Fe_3O_4/GCE in 0.1 M PBS containing 5 mmol/L $[Fe(CN)_6]^{3-/4-}$ and 0.1 M KCl.

Further information based on 3D-HRGO/Fe_3O_4 electrochemical sensor test results was displayed in Supplementary materials (S.2).

3.4 Individual and simultaneous quantification of Cd^{2+}, Pb^{2+}, Cu^{2+}, and Hg^{2+}

Quantification of Cd^{2+}, Pb^{2+}, Cu^{2+}, and Hg^{2+} was implemented under the optimal testing conditions by using the DPASV method based on 3D-HRGO/Fe_3O_4 nanocomposite electrochemical sensor, and the results were shown in Fig. 3.

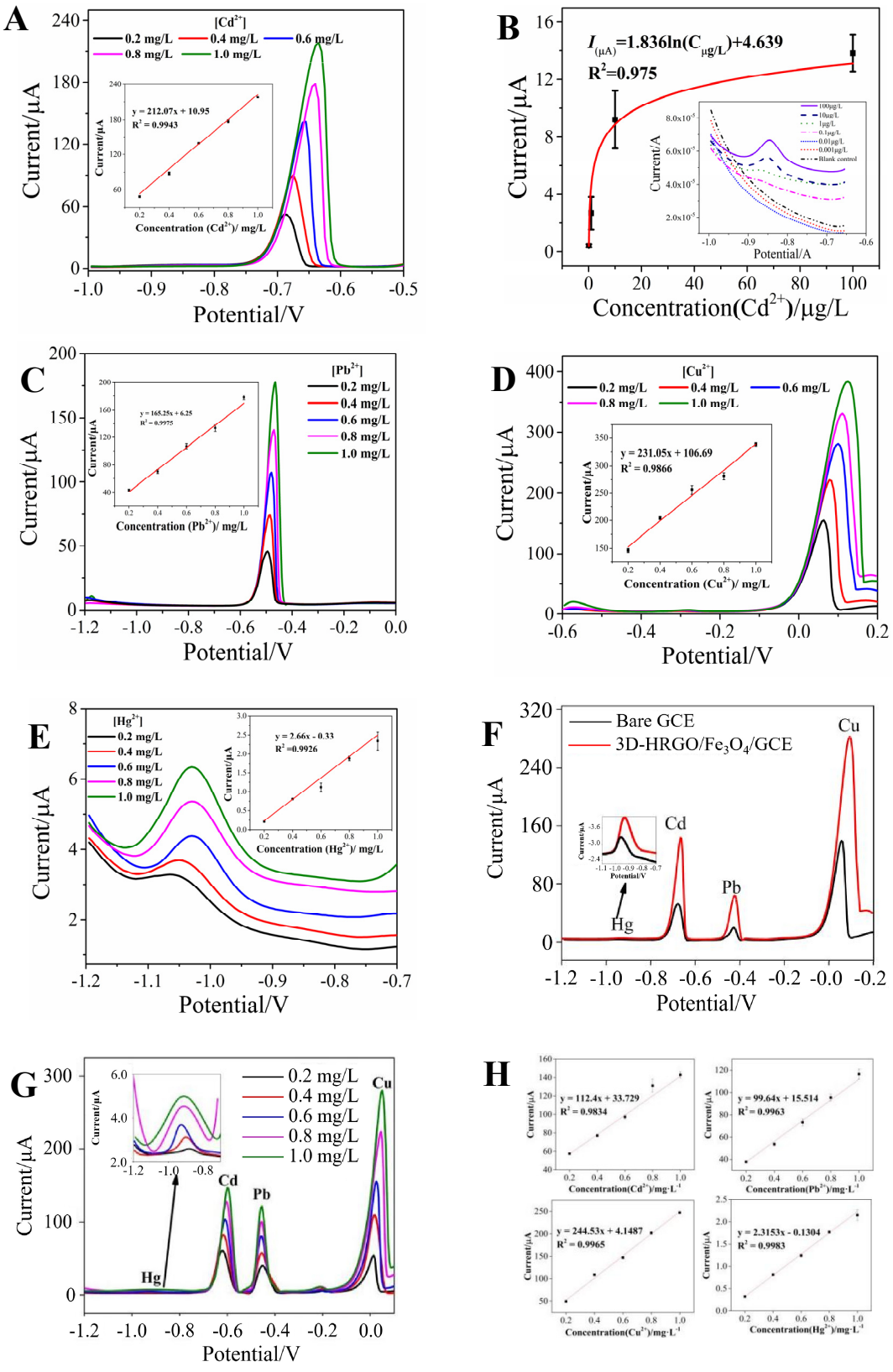

Fig. 3 Modified electrode performance of individual and simultaneous detection of Cd^{2+}, Pb^{2+}, Cu^{2+}, and Hg^{2+}; (A-E) 3D-HRGO/Fe_3O_4/GCE for individual detection of Cd^{2+}, Pb^{2+}, Cu^{2+}, and Hg^{2+} in a 0.1 M PBS and linear fit concentration and response current (pH 5.0) (Incr E: 0.005 v, amplitude: 0.05 v, pulse width:0.05 s, pulse period (sec) = 0.5, deposition E: -1.4 v, deposition time: 180s, quiet time: 5 s); (F) 3D-HRGO/Fe_3O_4/GCE and bare GCE for simultaneous detection of 0.8 mg/L Cd^{2+}, Pb^{2+}, Cu^{2+}, and Hg^{2+}; (G) 3D-HRGO/Fe_3O_4/GCE for simultaneous detection of Cd^{2+}, Pb^{2+}, Cu^{2+}, and Hg^{2+}; (H) The linear fit for 3D-HRGO/Fe_3O_4/GCE simultaneous detection of Cd^{2+}, Pb^{2+}, Cu^{2+} and Hg^{2+}.

Fig. 3A-E indicated the individual detection of Cd^{2+}, Pb^{2+}, Cu^{2+} and Hg^{2+}. Interestingly, compared to the simultaneous detection, where a universal conclusion can be summed up is that the response current for each metal of individual detection is much stronger. What can we infer is that the reduction of metal ions on the electrode is competitive. Before the simultaneous detection, the oxide peaks for each metal ion were tested and located at -0.76 V (Cd^{2+}), -0.43 V (Pb^{2+}), 0.08 V (Cu^{2+}), and -0.95 (Hg^{2+}) V, respectively (Fig. 3F). As it shown in graphics, oxidation peaks of different heavy metal ions are quite well separated and the current responses are stronger on 3D-HRGO/Fe_3O_4/GCE, which proves that the modified electrochemical sensor has abilities to improve the sensitivity. In the simultaneous detection test, the current-potential response curves corresponding to different concentrations are shown in Fig. 3G. In the range of (200 –1000) μg/L for Cd^{2+}, Pb^{2+}, Cu^{2+} and Hg^{2+}, the linear equations are $y = 112.4x + 33.729$ ($R^2 = 0.9834$), $y = 99.64x + 15.514$($R^2 = 0.9963$), $y = 244.53x + 4.1487$ ($R^2 = 0.9965$), $y = 2.3153x + 0.1304$ ($R^2 = 0.9983$), respectively (Fig. 3H); The LOD (S/N = 3) are 0.1 μg/L, 0.6 μg/L, 0.6 μg/L and 0.9 μg/L for Cd^{2+}, Pb^{2+}, Cu^{2+} and Hg^{2+} in simultaneous detection, respectively. Furthermore, in contrast to the simultaneous detection, a further individual detection was conducted specifically for Cd^{2+} to explore the LOD for individual detection, revealing a significant result (Fig. 3B). This experiment yielded a realistic LOD of 0.1 μg/L and nonlinear correlation equation: $I = 1.863\ln[Cd^{2+}]+4.639$, $R^2 = 0.975$. Applying the same method for the individual detection of Pb^{2+}, Cu^{2+}, and Hg^{2+}, LODs of 0.2 μg/L, 0.2 μg/L, and 0.4 μg/L were obtained, respectively.

The repeatability, reproducibility, and recovery results of 3D-HRGO/Fe_3O_4 nanocomposite-based electrochemical sensor for individual and simultaneous detection of Cd^{2+}, Pb^{2+}, Cu^{2+} and Hg^{2+} are presented in S. 3 and S. 4. In an individual detection of heavy metal test where the values of relative standard deviations (RSDs) for repeatability, reproducibility, and recoveries are 0.95%, 2.56%, and 95.7% – 109%. In a simultaneous detection where the values of RSDs for repeatability and reproducibility are within 5%. Nevertheless, no matter whether in individual or simultaneous detection, the 3D-HRGO/Fe_3O_4/GCE exhibited an excellent anti-interference capability (S. 3 A-B and S. 4 A-B).

For comparison, the results for the detection of Cd^{2+}, Pb^{2+}, Cu^{2+}, and Hg^{2+} using 3D-HRGO/Fe_3O_4 nanocomposite-based electrochemical sensors and other reported electrochemical sensors are shown in Table 1. The proposed method has higher sensitivity and a wider linear range than most other electrochemical methods. Also, it is more convenient because of the simultaneous detection of multiple heavy metals.

3.5 Simultaneous quantification of Cd^{2+}, Pb^{2+}, Cu^{2+}, and Hg^{2+} in edible mushrooms

The electrochemical sensor, based on the developed 3D-HRGO/Fe_3O_4 nanocomposite, was utilized for the detection of Cd^{2+}, Pb^{2+}, Cu^{2+}, and Hg^{2+} in various edible mushroom samples, including *L. edodes*, *T. fuciformis*, and *A. blazei*, employing the DPASV method. The obtained results are presented in Table 2. Additionally, the AAS/AFS methods were employed for the simultaneous detection of Cd^{2+}, Pb^{2+}, Cu^{2+}, and Hg^{2+}, and the corresponding results are also displayed in Table 2. Notably, there was no significant disparity observed between the proposed DPASV method and the conventional methods. The RSDs are within 5%, which means the method we developed is acceptable and these results are credible.

Table 1 Comparison of analytical performance over various modified electrodes.

Electrodes	Linear range (μg/L)				Detection limit (μg/L)				Detection Mode	Ref.
	Cd^{2+}	Pb^{2+}	Cu^{2+}	Hg^{2+}	Cd^{2+}	Pb^{2+}	Cu^{2+}	Hg^{2+}		
FET/RGO	--	--	--	--	--	-	--	0.2	individual	[36]
Poly/GO/GCE	8 -12000	4 -4000	--	--	1.0	1.2	--	--	simultaneous	[37]
MB/RGO/GCE	8 -3000	8 -3000	--	--	2	1.3	--	--	simultaneous	[38]
Bi/TRGO/GCE	1 -120	1 -120	--	--	0.4	1.0	--	--	simultaneous	[39]
$NiCo_2O_4$/PPy/3D-RGO/GCE	--	3 -150	--	--	--	0.04	--	--	individual	[40]
ITO/RUT/CH/GCE	0.9 -42	2 -60	--	--	0.1	1.7	--	--	individual	[41]
DTB/RGO/GCE	--	0.1 -1000	--	--	--	0.08	--	--	individual	[42]
ZnO-L-cys/GCE	--	10 -140	--	--	--	0.397	--	--	individual	[43]
Nano-Ag/CPE	5 -160	5 -160	--	--	90	48	--	--	simultaneous	[44]
CNTs-MOFs/GCE	30 -17000	--	--	--	22	--	--	--	individual	[45]
$Co_2Mn_2O_4$/GCE	--	2 -180	--	--	--	0.83	--	--	individual	[46]
ZIF-67/MWCNT/Nafion/GCE	--	0.3 -1000	0.08 -320	--	--	0.21	0.064	--	simultaneous	[47]
GQDs/Nafion/GCE	20 -200	20 -200	--	--	11.3	8.49	--	--	simultaneous	[48]
3D-HRGO/Fe_3O_4/GCE	0.1 -1000	--	--	--	0.1	0.2	0.2	0.4	individual	This
	200 -1000	200 -1000	200 -1000	200 -1000	0.1	0.6	0.6	0.9	simultaneous	work

Table 2 Quantification of heavy metals in mushrooms by both the proposed method and the national standard method (AAS/AFS).

Samples	3D-HRGO/Fe_3O_4/GCE (DPASV) (mg/kg)				National Food Safety Standard (AAS/AFS) (mg/kg)				The RSD between DPASV &AAS/AFS
	Cd^{2+}	Pb^{2+}	Cu^{2+}	Hg^{2+}	Cd^{2+}	Pb^{2+}	Cu^{2+}	Hg^{2+} (AFS)	
L. edodes. 1	0.043±0.001	0.082±0.001	0.013±0.002	0.015±0.002	0.042±0.008	0.079±0.031	0.016±0.010	0.012±0.000	1.6% – 4.5%
L. edodes. 2	0.049±0.002	0.046±0.002	0.005±0.001	0.031±0.003	0.048±0.002	0.045±0.013	0.048±0.006	0.030±0.004	1.4% – 2.3%
L. edodes. 3	0.046±0.003	0.060±0.009	0.076±0.007	0.033±0.001	0.046±0.010	0.056±0.016	0.075±0.009	0.033±0.003	0.9% – 4.8%
L.edodes. 4	0.042±0.003	0.064±0.003	0.031±0.001	0.030±0.006	0.040±0.007	0.067±0.028	0.029±0.002	0.028±0.001	3.2% – 4.8%
T. fuciformis. 1	0.010±0.001	0.040±0.008	0.220±0.008	0.021±0.003	0.009±0.001	0.035±0.033	0.210±0.013	0.020±0.012	3.2% – 3.6%
T. fuciformis. 2	0.008±0.001	0.051±0.002	0.470±0.008	0.010±0.001	0.007±0.003	0.053±0.033	0.470±0.091	0.010±0.002	0.1% – 3.6%
A. blazei. 1	0.680±0.002	0.150±0.006	12.000±0.190	0.063±0.001	0.700±0.014	0.150±0.027	12.000±0.370	0.063±0.025	0.1% – 2.0%
A. blazei. 2	0.450±0.001	0.130±0.001	0.450±0.004	0.052±0.001	0.460±0.031	0.120±0.064	0.450±0.150	0.052±0.019	0.1% – 2.7%

Description: According to the GB 2762-2022. National food safety standard: Limit of pollutants in food that give a limit content of heavy metals in fresh mushroom (*L. edodes* and *A. blazei*) and dried mushroom (*T. fuciformis*), the data of Cd^{2+}, Pb^{2+}, Cu^{2+}, Hg^{2+} shown above was obtained from dried mushrooms powder has been transformed to a standard value.

As it is known that Cd^{2+}, Pb^{2+}, and Hg^{2+} are common contaminants in edible mushrooms, could be enriched in the human body through the food chain and damaging human health. According to current Chinese national standards GB 2762-2022 (National Standard for Food Safety Limits of Contaminants in Foods)[53], the limits of these food contaminants are as follows: the limits of Cd^{2+}, Pb^{2+}, and Hg^{2+} in *L. edodes* are 0.5 mg/kg, 0.3 mg/kg, and 0.1 mg/kg, and in *A. blazei* are 1.0 mg/kg, 1.0 mg/kg, and 0.1 mg/kg(by fresh weight), the limits of Cd^{2+}, Pb^{2+}, and Hg^{2+} in *T. fuciformis* are 0.5 mg/kg, 1.0 mg/kg, and 0.1 mg/kg (by dry weight). The edible mushrooms purchased from the local markets had been tested and the results showed no heavy metal ions (Cd^{2+}, Pb^{2+}, and Hg^{2+}) beyond the limitation. Nevertheless, here some important disputations should be clarified regarding the definitions of heavy metal ions and food pollutants. It is well known that Cu^{2+} belongs to heavy metal, and it was defined as a pollutant in food in past years until it was abolished in 2010 in China, but an overdose of Cu^{2+} could be a potential risk to human health[54].

4. Conclusions

A 3D-HRGO/Fe_3O_4 nanocomposite was synthesized to develop a novel electrochemical modified electrode for simultaneous quantification of trace heavy metals in edible mushrooms combined with the DPASV method. In this study, unlike general researches where graphene oxide was as a usual material with hydrophilicity and easily dispersed in aqueous, but with much lower conductivity. So, how to make graphene with highly reduction status for keeping high conductivity and find a proper dispersing system? Here in this research, a simple and environmental friendly aqueous solution 75% ethanol-0.1% Nafion was applied to adapt the super hydrophobic 3D-HRGO/Fe_3O_4. Compared to others sensors, 3D-HRGO/Fe_3O_4/GCE obtained the best response signal, which means the lower detection can it realize. Thus, the proposed electrochemical method exhibits obvious advantages for simultaneous detection of trace Cd^{2+}, Pb^{2+}, $Cu^{2+}$and Hg^{2+}. It is more sensitive and convenient compared to other similar electrochemical methods, as well as good repeatability, reproducibility, and recovery. The detection limit for Cd^{2+}, Pb^{2+}, Cu^{2+} and Hg^{2+} are low to 0.1 μg/L, 0.6 μg/L, 0.6 μg/L and 0.9 μg/L, respectively. The proposed method was used to detect Cd^{2+}, Pb^{2+}, $Cu^{2+}$and Hg^{2+} in edible mushrooms. The results are in good agreement with the standard method. It indicates that the 3D-HRGO/Fe_3O_4 nanocomposite-based DPASV electrochemical sensor provides an accurate, sensitive, and convenient tool to realize simultaneous and rapid quantification of Cd^{2+}, Pb^{2+}, $Cu^{2+}$and Hg^{2+} in edible mushrooms. It is promising to develop a portable device for the detection of heavy metal contamination in edible resources on-site.

Acknowledgments

Partial support of this research by the National Natural Science Foundation of China (31972173), the Program for Science & Technology Innovation Talents of Hunan Province (2022SK2100, 2021RC4032, and 2019TP1029), and the Ministry of Agriculture of the People's Republic of China (GJFP2021) is gratefully acknowledged.

Declaration of Conflicting Interest

All authors declared that no potential conflicts of interest to the research.

References

[1] J. Falandysz, J. Zhang, M. Mędyk, et al., Mercury in stir-fried and raw mushrooms from the Boletaceae family from the geochemically anomalous region in the Midu county, China, Food Control 102 (2019) 17–21. https://doi.org/10.1016/j.foodcont.2019.03.007.

[2] M. Dowlati, H.R. Sobhi, A. Esrafili, et al. Heavy metals content in edible mushrooms: A systematic review, meta-analysis, and health risk assessment. Trends in Food Science & Technology 109 (2021) 527–535. https://doi.org/10.1016/j.tifs.2021.01.064.

[3] M.S. Islam, M.K. Ahmed, M. Raknuzzaman, et al., Heavy metal pollution in surface water and sediment: A preliminary assessment of an urban river in a developing country, Ecological Indicators 48 (2015) 282–291. https://doi.org/10.1016/j.ecolind.2014.08.016.

[4] D. Tibebe, M. Hussen, M. Mulugeta, et al. Assessment of selected heavy metals in honey samples using flame atomic absorption spectroscopy (FAAS), Ethiopia, BMC Chemistry 16 (2022) 87. https://doi.org/10.1186/s13065-022-00878-y.

[5] M.J. Zhang, H.F. Shang, J.J. Shang, et al. Spectroscopic methods for isotope analysis of heavy metal atoms: A review, Spectrochimica Acta Part B: Atomic Spectroscopy 207 (2023) 106740. https://doi.org/10.1016/j.sab.2023.106740.

[6] C. Stihi, Popescu I V, M. Frontasyeva, et al., Characterization of Heavy Metal Air Pollution in Romania Using Moss Biomonitoring, Neutron Activation Analysis, and Atomic Absorption Spectrometry, Analytical Letters 50 (2017) 2851–2858. https://doi.org/10.1080/00032719.2016.1275661.

[7] E. Covaci, M. Senila, M. Ponta, et al., Mercury speciation in seafood using non-chromatographic chemical vapor generation capacitively coupled plasma microtorch optical emission spectrometry method - Evaluation of methylmercury exposure, Forest Policy and Economics 82 (2017) 266–273. https://doi.org/10.1016/j.foodcont.2017.07.006.

[8] S. Butaciu, T. Frentiu, M. Senila, et al., Determination of Cd in food using an electrothermal vaporization capacitively coupled plasma microtorch optical emission microspectrometer: Compliance with European legislation and comparison with graphite furnace atomic absorption spectrometry, Food Control 61 (2016) 227–234. https://doi.org/10.1016/j.foodcont.2015.09.040.

[9] T. Thabit, S.A. Shokr, D. Elgeddawy, et al., Determination of heavy metals in wheat and barley grains using ICP-MS/MS, Journal of AOAC international 103 (2020) 1277–1281. https://doi.org/10.1093/jaoacint/qsaa029.

[10] S. Moussa, J. Mauzeroll, Review—Microelectrodes: An Overview of Probe Development and Bioelectrochemistry Applications from 2013 to 2018, Journal of the Electrochemical Society 166 (2019) G25–G38. https://doi.org/10.1149/2.0741906jes.

[11] M. Tarapoulouzi., V. Ortone, S. Cinti, Heavy metals detection at chemometrics-powered electrochemical (bio) sensors, Talanta 12 (2023) 123410. https://doi.org/10.1016/j.talanta.2022.123410.

[12] D. Shi, W. Wu, X. Li, Ultrasensitive detection of mercury(II) ions on a hybrid film of a graphene and gold nanoparticle-modified electrode, Analytical Methods 14 (2022) 2161–2167. https://doi.org/10.1039/d2ay00413e.

[13] F. Pogăcean, C. Varodi, L. Măgeruşan, et al., Highly sensitive electrochemical detection of azithromycin with graphene-modified electrode, Sensors 22 (2022) 6181. https://doi.org/10.3390/s22166181

[14] T. Wang, D. Huang, Z. Yang, et al., A Review on Graphene-Based Gas/Vapor Sensors with Unique Properties and Potential Applications, Nano-Micro Letters 8 (2016) 95-119. https://doi.org/10.1021/nl801412y.

[15] X. Yu, H. Cheng, M. Zhang, et al., Graphene-based smart materials, Nature Reviews Materials 2 (2017) 17046. https://doi.org/10.1038/natrevmats.2017.46.

[16] J. Park, Y.S. Cho, S.J. Sung, et al., Characteristics tuning of graphene-oxide-based-graphene to various end-uses, Energy Storage Materials 14 (2018) 8-21. https://doi.org/10.1016/j.ensm.2018.02.013.

[17] I. Shtepliuk, N.M. Caffrey, T. Iakimov, et al., On the interaction of toxic Heavy Metals (Cd, Hg, Pb) with graphene quantum dots and infinite graphene, Scientific Reports 7 (2017) 3934. https://doi.org/10.1038/s41598-017-04339-8.

[18] A. Alazmi, O.E. Tall, S. Rasul, et al. A process to enhance the specific surface area and capacitance of hydrothermally reduced graphene oxide, Nanoscale, 41 (2016) 17782–17787. https://doi.org/10.1039/c6nr04426c.

[19] Z. Z. Alisultanov, I. K. Kamilov, Transport properties of epitaxial graphene formed on the surface of a metal, Physics of the Solid State 56 (2014) 854–864. https://doi.org/10.1134/s1063783414040027.

[20] Y.W. Tan, J.W. Jiang, Effect of interlayer space on the structure and Poisson's ratio of a graphene/MoS_2 tubular van der Waals heterostructure, Journal of Applied Physics 124 (2018) 084302. https://doi.org/10.1063/1.5037392.

[21] Muqiu Wu, Rong An, Sudheer Kumar Yadav, et al., Graphene tailored by Fe_3O_4 nanoparticles: low-adhesive and durable superhydrophobic coatings, RSC Advances 9 (2019) 16235–16245. https://doi.org/10.1039/c9ra02008j.

[22] Y. Yang, Y.C. Zou, C.R. Woods, et al., Stacking Order in Graphite Films Controlled by Van der Waals Technology, Nano Letters 19 (2019) 8526-8532. https://doi.org/10.1021/acs.nanolett.9b03014.

[23] Z. Chen, W. Ren, L. Gao, et al., Three-dimensional flexible and conductive interconnected graphene networks grown by chemical vapor deposition, Nature Materials 10 (2011) 424-428. https://doi.org/10.1038/nmat3001.

[24] Y. Wei, C. Gao, F.L. Meng, et al., SnO_2/Reduced graphene oxide nanocomposite for the simultaneous electrochemical detection of Cadmium (II), Lead(II), Copper(II), and Mercury(II): An Interesting Favorable Mutual Interference, Journal of Physical Chemistry C 116 (2012) 1034–1041. https://doi.org/10.1007/s10853-016-0650-9.

[25] D. Manoj, S. Rajendran, T. Hoang, et al., In-situ growth of 3D Cu-MOF on 1D halloysite nanotubes/reduced graphene oxide nanocomposite for simultaneous sensing of dopamine and paracetamol, Journal of Industrial and Engineering Chemistry112 (2022) 287–295. https://doi.org/10.1016/j.jiec.2022.05.022.

[26] R. Zokhtareh, M. Rahimnejad, H. Karimi-Maleh, et al., A novel sensing platform for electrochemical detection of metronidazole antibiotic based on green-synthesized magnetic Fe_3O_4 nanoparticles, Environmental Research 216 (2023) 114643. https://doi.org/10.1016/j.envres.2022.114643.

[27] R. Zokhtareh, M. Rahimnejad, H. Karimi-Maleh, et al., A new approach to electrochemical sensing of a wildly used antibiotic; ciprofloxacin, Measurement 215 (2023) 112872. https://doi.org/10.1016/j.measurement.2023.112872.

[28] S. Park, J. An, J.R. Potts, et al., Hydrazine-reduction of graphite and graphene oxide, Carbon 49 (2011) 3019–3023. https://doi.org/10.1016/j.carbon.2011.02.071.

[29] C. Lou, T. Jing, J. Tian, et al., Hou, J. Fan, Z. Guo, 3-Dimensional graphene/Cu/Fe_3O_4 composites: Immobilized laccase electrodes for detecting bisphenol A, Journal of Materials Research 34 (2019) 2964–2975. https://doi.org/10.1557/jmr.2019.248.

[30] N. Sarlak, T.J. Meyer, Fabrication of completely water soluble graphene oxides graft poly citric acid using different oxidation methods and comparison of them, Journal of Molecular Liquids 243 (2017) 654–663. https://doi.org/10.1016/j.molliq.2017.08.086.

[31] M. Soylak, H. Colak, M. Tuzen, et al., Comparison of digestion procedures on commercial powdered soup samples for the determination of trace metal contents by atomic absorption spectrometry, Journal of Food and Drug Analysis 14 (2020). https://doi.org/10.38212/2224-6614.2500.

[32] A.V. Alaferdov, R. Savu, C. Fantini, et al., Raman spectra of multilayer graphene under high temperatures, Journal of Physics: Condensed Matter 32 (2020) 385704. https://doi.org/10.1088/1361-648X/ab95ce.

[33] S. Stankovich, D.A. Dikin, R.D. Piner, et al., Synthesis of graphene-based nanosheets via chemical reduction of exfoliated graphite oxide, Carbon, 45 (2007) 1558–1565 2007. https://doi.org/10.1016/j.carbon.2007.02.034.

[34] L.P. Bakos, L. Sárvári, K. László, et al., Electric and Photocatalytic Properties of Graphene Oxide Depending on the Degree of Its Reduction, Nanomaterials 10 (2020) 2313. https://doi.org/10.3390/nano10112313.

[35] M.K. Rabchinskii, S.A. Ryzhkov, D.A. Kirilenko, et al., From graphene oxide towards aminated graphene: facile synthesis, its structure, and electronic properties, Scientific Reports 10 (2020) 6902. https://doi.org/10.1038/s41598-020-63935-3.

[36] Z. Z. Zhang, J. X. Zhang, Z. H. Guo, et al., Effect of graphene liquid crystal on dielectric properties of polydimethylsiloxane nanocomposites, Composites Part B: Engineering 176 (2019) 107338. https://doi.org/10.1016/j.compositesb.2019.107338.

[37] J. X. Zhang, P. P. Li, Z. Z. Zhang, et al., Solvent-free graphene liquids: Promising candidates for lubricants without the base oil, Journal of Colloid and Interface Science 542 (2019) 159–167. https://doi.org/10.1016/j.jcis.2019.01.135.

[38] C. Q. Lou, T. Jing, Z. H. Guo, et al., 3-Dimensional graphene/Cu/Fe_3O_4 composites: Immobilized laccase electrodes for detecting bisphenol A, Journal of Materials Research 34 (2019) 2964–2975. https://doi.org/10.1557/jmr.2019.248.

[39] H. Y. Li, Z. R. He, D. W. Li, et al., Modifying Electrical and Magnetic Properties of Single-Walled Carbon Nanotubes by Decorating with Iron Oxide Nanoparticles, Journal of Nanoscience and Nanotechnology 20 (2020) 2611–2616. https://doi.org/.

[40] H.G. Sudibya, Q. He, H. Zhang, P. Chen, et al., Electrical Detection of Metal Ions Using Field-Effect Transistors Based on Micropatterned Reduced Graphene Oxide Films, ACS Nano 5 (2011) 1990–1994. https://doi.org/10.1021/nn103043v.

[41] M. Chen, M. Chao, X. Ma, et al., Poly (crystal violet)/graphene-modified electrode for the simultaneous determination of trace lead and cadmium ions in water samples, J Appl Electrochem 44 (2014) 337–344. https://doi.org/10.1007/s10800-013-0641-3.

[42] K. Keawkim, S. Chuanuwatanakul, O. Chailapakul, S. Motomizu, Determination of lead and cadmium in rice samples by sequential injection/anodic stripping voltammetry using a bismuth film/crown ether/Nafion modified screen-printed carbon electrode, Food Control 31 (2013) 14–21. https://doi.org/10.1016/j.foodcont.2012.09.025.

[43] X. Xuan, M. F. Hossain, J. Y. Park, A fully integrated and miniaturized heavy metal detection sensor based on micro-patterned reduced graphene oxide. Scientific Reports 6 (2016) 33125. https://doi.org/10.1038/srep33125.

[44] X. Wei, C. Wang, P. Dou, et al., Synthesis of $NiCo_2O_4$ nanoneedle@polypyrrole arrays supported on 3D graphene electrode for high-performance detection of trace Pb^{2+}, J Material Science 52 (2017) 3893–3905. https://doi.org/10.1007/s10853-016-0650-9.

[45] B. Dalkıran, Amperometric determination of heavy metal using an HRP inhibition biosensor based on ITO nanoparticles-ruthenium (III) hexamine trichloride composite: Central composite design optimization, Bioelectrochemistry 135 (2020) 107569. https://doi.org/10.1016/j.bioelechem.2020.107569.

[46] Y. Li, R. Cui, H. Huang, J. Dong, et al., High performance determination of Pb^{2+} in water by 2,4-dithiobiuret-Reduced graphene oxide composite with wide linear range and low detection limit, Analytica Chimica Acta 1125 (2020) 76–85. https://doi.org/10.1016/j.aca.2020.05.036.

[47] V.H.B. Oliveira, F. Rechotnek, E.P. Da Silva, et al., A sensitive electrochemical sensor for Pb^{2+} ions based on ZnO nanofibers functionalized by L-cysteine, Journal of Molecular Liquids 309 (2020) 113041. https://doi.org/10.1016/j.molliq.2020.113041.

[48] M. Amare, A. Worku, A. Kassa, W. Hilluf, et al., Green synthesized silver nanoparticle modified carbon paste electrode for SWAS voltammetric simultaneous determination of Cd (II) and Pb (II) in Bahir Dar Textile discharged effluent, Heliyon 6 (2020) e04401. https://doi.org/10.1016/j.heliyon.2020.e04401.

[49] L. Yu, J. W. Wan, X. Z. Meng, et al., A simple electrochemical method for Cd (II) determination in real samples based on carbon nanotubes and metal-organic frameworks, International Journal of Environmental Analytical Chemistry 102 (2022) 4757–4767. https://doi.org/10.1080/03067319.2020.1789611.

[50] N. Bashir, M. Akhtar, H.Z.R. Nawaz, et al., A high performance electrochemical sensor for Pb^{2+} ions based on carbon nanotubes functionalized $CoMn_2O_4$ nanocomposite, Chemistry Select 5 (2020) 7909–7918. https://doi.org/10.1002/slct.202001393.

[51] Y. Zhang, H. Yu, T. Liu, et al., Highly sensitive detection of Pb^{2+} and Cu^{2+} based on ZIF-67/MWCNT/Nafion-modified glassy carbon electrode, Analytica Chimica Acta 1124 (2020) 166–175. https://doi.org/10.1016/j.aca.2020.05.023.

[52] J. Pizarro, R. Segura, D. Tapia, F. Navarro, et al., Inexpensive and green electrochemical sensor for the determination of Cd (II) and Pb (II) by square wave anodic stripping voltammetry in bivalve mollusks, Food Chemistry 321 (2020) 126682. https://doi.org/10.1016/j.foodchem.2020.126682.

[53] GB 2762-2022. National food safety standard: Limit of pollutants in food. National Health Commission of the People's Republic of China, the State Administration of Market Supervision, 2022. http://down.foodmate.net/standard/sort/3/123275.html.

[54] H. Zhao, Y. Wang, D. Fei, et al., Xing, Destruction of redox and mitochondrial dynamics co-contributes to programmed cell death in chicken kidney under arsenite or/and copper (II) exposure, Ecotoxicology and Environmental Safety 179 (2019) 167–174. https://doi.org/10.1016/j.ecoenv.2019.04.062.